Int. J. Electrochem. Sci., 11 **(2016)** 7922 – 7933, doi: 10.20964/2016.09.59

International Journal of
ELECTROCHEMICAL
SCIENCE
www.electrochemsci.org

A Study of the Electrochemical Performance of Strip Supercapacitors under Bending Conditions

Ruirong Zhang[1,*], *Yanmeng Xu*[1,*], *David Harrison*[1], *John Fyson*[1] *and Darren Southee*[2]

[1] Cleaner Electronics Group, College of Engineering, Design and Physical Sciences, Brunel University London, Uxbridge, UK
[2] Loughborough Design School, Loughborough University, Leicestershire, UK
[*]E-mail: ruirong.zhang@brunel.ac.uk; yanmeng.xu@brunel.ac.uk

Received: 6 May 2016 / *Accepted:* 18 July 2016 / *Published:* 7 August 2016

In recent years, much effort has been spent developing thin, lightweight and flexible energy storage devices to meet the various requirements of modern smart electronics. In this work, thin strip supercapacitors were successfully developed using activated carbon as the active electrode material. The electrochemical performance of these strip supercapacitors has been studied under mechanical bending conditions. The results indicate that the strip supercapacitor was functional under bending conditions between the bending angles of 30° to 150°. The capacitance of the sample was still about 70% of the original capacitance at different bending angles. This suggests the strip supercapacitor developed has a reasonable flexibility. Simulation model of equivalent circuit was established to analyze the charge transfer resistance (CTR) and equivalent series resistance (ESR) results in electrochemical impedance spectroscopy (EIS) testing. The correlation between the capacitance and the resistance of the strip supercapacitor under bending conditions was investigated and obtained.

Keywords: Flexible; Strip supercapacitors; Bending conditions

1. INTRODUCTION

Supercapacitors, also named electrochemical capacitors, have attracted great attention because of their high power density, long life cycle and high efficiency. Compared with rechargeable batteries and conventional capacitors, supercapacitors can store large amounts of energy and provide high power, bridging the property gap of batteries and capacitors. Recently, supercapacitors have been used as energy sources for rapid energy storage and power delivery in consumer electronics, electric vehicles and emergency power supplies [1-4]. Because of the different charge storage mechanism, supercapacitors can be classified into pseudocapacitors and electrical double-layer capacitors (EDLCs)

[5-8]. The energy is stored in an EDLC by charge separation at the interface between the surface of a conductive electrode and an electrolyte. Because of their large surface area, porous carbon materials are widely used for the electrode materials in EDLCs as they can provide a large surface area to store the electrical charges [3, 6, 9-11].

In order to meet requirements for wearable and portable electronic devices, supercapacitors are being developed to be thinner and lighter. However, many current supercapacitors are still too bulky, rigid and heavy for flexible energy storage applications [12, 13]. It is a challenge to achieve highly efficient miniaturized supercapacitors, such as flexible supercapacitors, which can be used in wearable and portable electronics. Recently, some efforts have been made to develop the flexible supercapacitors [12-15]. Pushparaj et al. [12] developed single contiguous nanocomposite units that can be used as building blocks for flexible energy storage devices. These single contiguous units were made by using nanoporous cellulose paper embedded with aligned carbon nanotube electrodes and electrolyte. Kaempgen et al. [14] fabricated film supercapacitors based on single-walled carbon nanotubes (SWCNTs) networks in combination with a printable gel electrolyte. Wang et al. [15] produced all-solid-state flexible micro-supercapacitors (MSC) on a chip based on Polyaniline (PANI) nanowire arrays. The MSC exhibited a good capacitance, fast rate capability and lower leakage current. In this work, strip EDLCs with a simple structure were fabricated by using activated carbon as the electrode material. The electrochemical performance of the strip supercapacitors under different bending angles was investigated.

2. EXPERIMENTAL

2.1 Typical structure of EDLCs

It is known that the energy is stored in EDLCs by the accumulation of charges at the boundary layer between the electrode and electrolyte. Based on the working mechanism of EDLCs, the strip supercapacitors were designed [1]. As shown in Fig. 1, the strip supercapacitor consists of two electrodes, a separator and electrolyte. The electrodes were made of activated carbon which provides a conductor with a high surface area, and separated by a layer of filter paper [16].

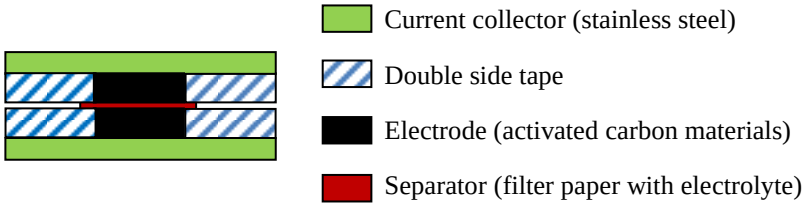

Figure 1. Schematic diagram of a cross-section of a typical strip supercapacitor.

2.2 Materials

Activated carbon powder (AC) and carboxymethyl cellulose (CMC) were purchased from

Sigma-Aldrich Company. The AISI 316L (Fe/Cr18/Ni10/Mo3) foil with the thickness of 0.05 mm was purchased from Advent Research Materials Company. Tetrabutylammonium tetrafluoroborate ($C_{16}H_{36}BF_4N$, 99%) and propylene carbonate ($C_4H_6O_3$) were both purchased from Sigma-Aldrich Company. Postlip filter papers (d=127 mm, the thickness is about 130 μm) were manufactured by Evans Adlard & Company Limited. All the materials above were used without further purification.

2.3 Manufacture of the strip supercapacitors

In this study, stainless steel strip was used as the current collector. Electrodes were made by coating a homogeneous AC slurry prepared by mixing AC with CMC binder solution on the 3 mm wide exposed surface of the stainless steel strip. More details can be found in the previous work published [16]. The organic electrolyte made by dissolving 1 M tetrabutylammonium tetrafluoroborate in propylene carbonate was dropped on the surface of the coated active materials of electrodes. These electrodes with the electrolyte were put in a vacuum desiccator at room temperature for 0.5 hours to allow the electrolyte to permeate well to the porous structure of the AC material. At the same time, the filter paper used as a separator was also fully wetted with the electrolyte. Finally, two electrodes with electrolyte separated by the separator were assembled to fabricate a strip supercapacitor as shown in Fig. 1, then the strip supercapacitor was sealed using a laminator to avoid the loss of electrolyte, using heat cured adhesive laminating film.

2.4 Experimental conditions, measurement and characterization

2.4.1 Reproducibility and bending test

In order to test the stability of the electrochemical performance of the EDLCs and the reproducibility, four samples were fabricated under the same conditions. The size of the electrode is 3×100 mm, the thickness of the electrode active materials is 375 μm, the binder content is 5% (based on the total weight of solids) and the electrolyte concentration is 1.0 mol/L. The sample for the bending test was made under the same processes as the samples used in reproducibility test but size of the electrode was larger (5×100 mm) in order to fit the experimental rig better.

2.4.2 Measurement and electrochemical performance characterization

The electrochemical performance of the EDLCs developed was studied by cyclic voltammetry (CV), galvanostatic charge-discharge test (GCD) and electrochemical impedance spectroscopy (EIS), using a VersaSTAT 3 electrochemical workstation.

The electrical capacitance of the supercapacitors could be calculated by the CV and GCD methods. Based on the CV curve, the capacitance, C1, can be calculated by the equation [17]:

$$C1 = \frac{Q_{total}/2}{\Delta V} \quad (1)$$

where Q_{total} is the supercapacitor's charge in coulombs, which is measured by the CV system used. ΔV is the voltage between the device's terminals in volts (V).

Based on the GCD curve, the capacitance, C2, can be directly calculated by the following equation:

$$C2 = \frac{i \times \Delta t}{\Delta V} \quad (2)$$

where *i* is the discharge current in amperes (*A*); ΔV is the voltage of the discharge (*V*).

3. RESULTS AND DISCUSSION

3.1 The reproducibility of the EDLCs

The EDLCs were characterized using CV and GCD test, and all the results are shown in Fig. 2 (a), (b) and (c). It can be found that the shapes of the four CV curves in Fig. 2 (a) are similar, and the areas of these curves are close. The shapes of all the GCD curves in Fig. 2 (b) are also similar, and there is only slight difference between the charge/discharge times in each curve. Fig. 2 (c) shows the comparison of the capacitances C1 and C2 calculated from the CV and GCD curves.

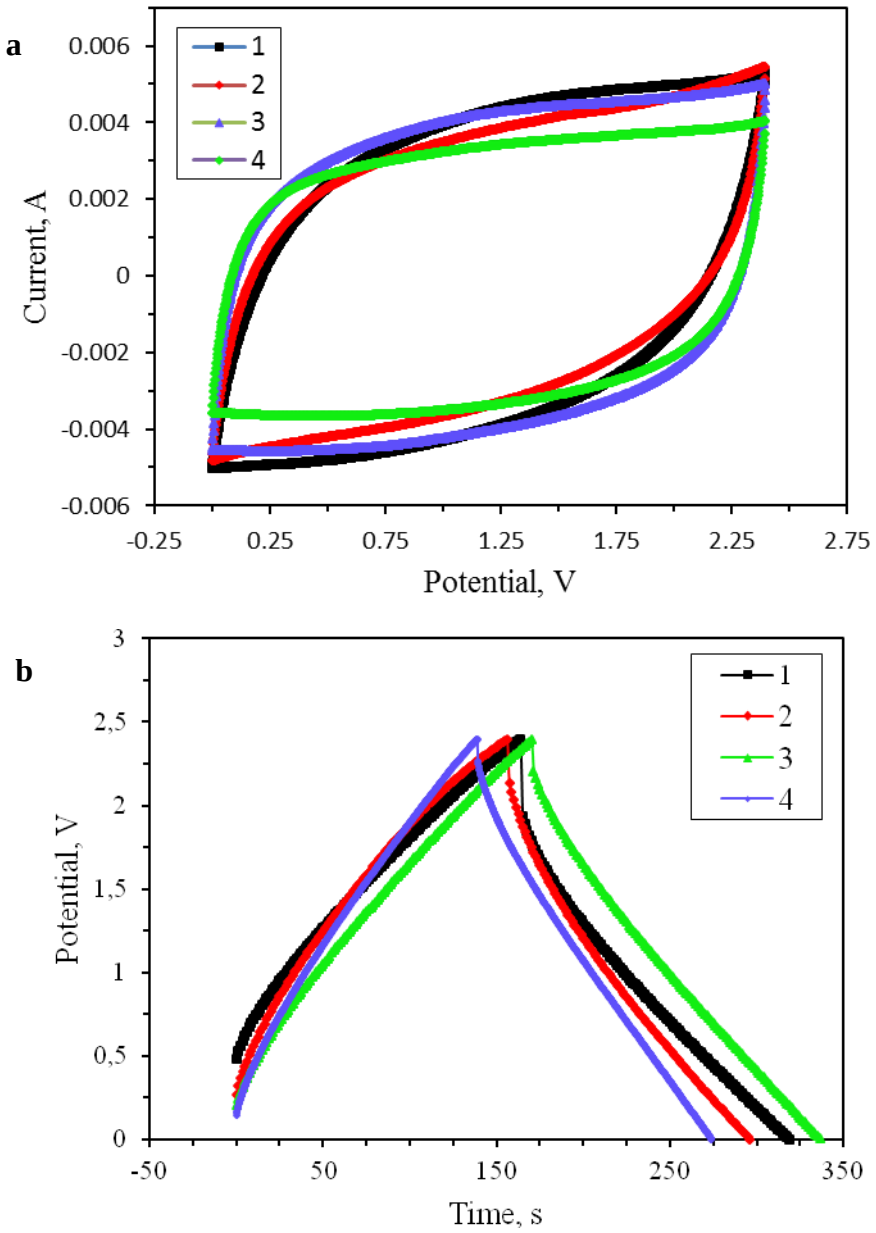

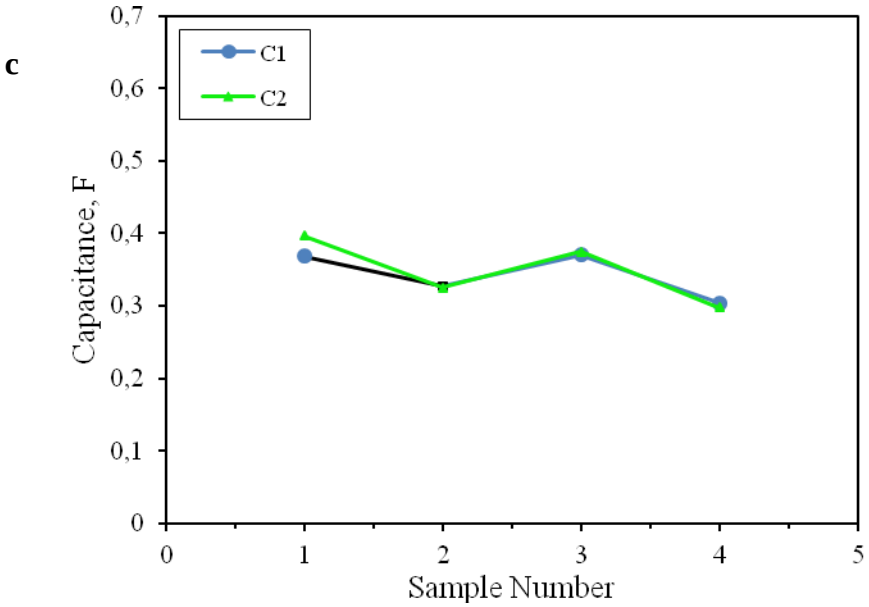

Figure 2. (a) CV and (b) GCD curves of of four samples with the same conditions, (c) the capacitances of the four samples obtained from CV curves (C1) and GCD curves (C2).

It is found that the C1 and C2 are close to each other, with the average value of 0.34 and 0.35 F, respectively. These results prove that the manufacturing processes for the strip EDLCs described above have a good reproducibility. Furthermore, it is obvious that there is only little difference between the two values of C1 and C2 for all the samples, i.e. the values of capacitance based on different tests change slightly. It indicates the capacitance measurement is reliable. Similar results were presented in other supercapacitors [18, 19], the values calculated form CV curves are nearly consistent with those obtained from the GCD measurement.

3.2 The electrochemical performance of the strip supercapacitor under the bending conditions

A new EDLC sample with the size of 5×100 mm was manufactured for the bending tests. The bending test was carried out as shown in the insert diagram on bottom right of Fig. 3. The electrochemical performance of the strip supercapacitor was investigated by CV, GCD and EIS test under different bending angles from 0° to 150°.

3.2.1 The electrochemical performance characterized by CV test

Fig. 3 also shows the CV curves of the strip supercapacitor sample measured at different bending angles, at the scan rate of 0.010 V/s. It can be seen that the shapes of the CV curves under the different bending conditions are similar. When the bending angle was at 30°, the area of the CV curve became smaller than that of the original sample (when the bending angle was 0°), indicating the corresponding capacitance (C1) decreased. When the bending angle increased to 60°, 90°, 120° and 150°, the area of the CV curves changed only slightly. This indicates there was no significant change

for the capacitances of the strip supercapacitor at different bending angles. This was very similar to the finding of the bending experiment for the flexible solid-state supercapacitors based on carbon nanoparticles/MnO_2 nanorods hybrid structure reported by Yuan et al. [20].

Table 1 shows C1 for this sample under the different bending angles calculated from the CV curves (Fig. 3) by Equation (1). The capacitance of this strip supercapacitor tested at the bending angle of 30° was equivalent to 68.5% of the original capacitance of this strip supercapacitor capacitance without bending. When the bending angle further increased to 60°, 90°, 120° and 150°, the capacitances changed slightly and fluctuated around 75% of the original capacitance.

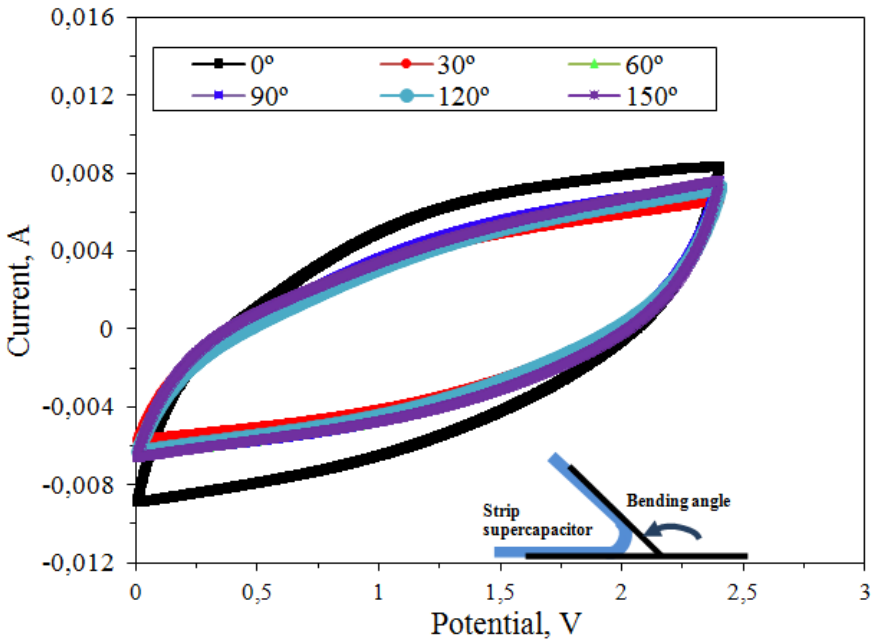

Figure 3. CV curves of a strip supercapacitor under different bending angles from 0-150°, and the insert is a diagram of the sample under the bending condition.

Table 1. Capacitances (C1) based on the CV curves (Fig. 3) for the sample under different bending angles.

Bending angle,°	C1, F	Percentage, %
0	0.537	100
30	0.368	68.5
60	0.408	76.0
90	0.416	77.4
120	0.391	72.8
150	0.411	78.5

3.2.2 The electrochemical performance characterized by GCD test

The GCD curves of the strip supercapacitor under different bending conditions are shown in Fig. 4. The shapes of the GCD curves recorded at different bending conditions are fairly similar.

However, the charge/discharge time decreased significantly when the bending angle increased from 0° to 30°. When the bending angle further increased to 60°, 90°, 120° and 150°, the charging/discharging time changed slightly. All the capacitances for this sample under different bending angles calculated from the GCD curves (Fig. 4) by Equation (2) were shown in Table 2. It is apparent that C2 decreased remarkably when the bending angle increased from 0° to 30°. When the bending angle further increased to 60°, 90°, 120° and 150°, the capacitance fluctuated around about 70% of the original capacitance.

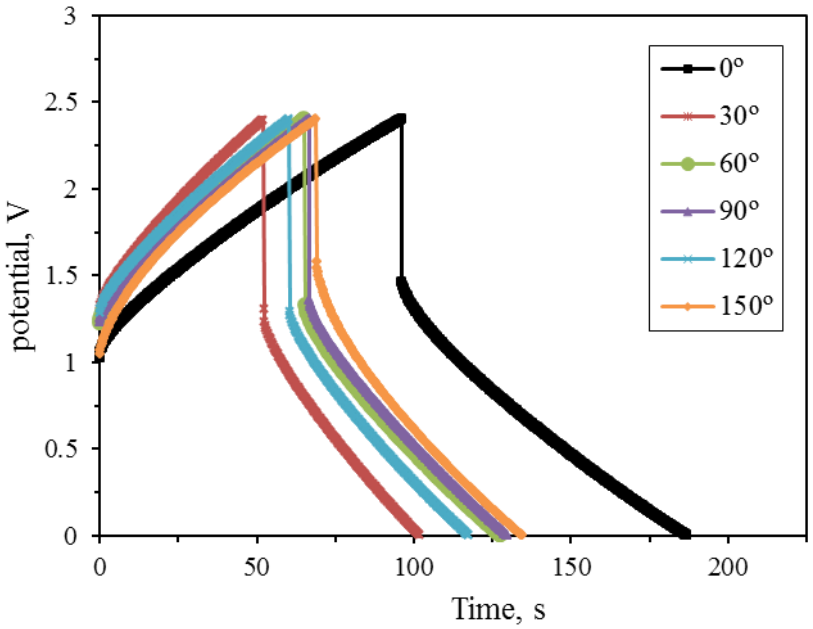

Figure 4. GCD curves of a strip supercapacitor at charging current of 0.010 A under different bending angles from 0-150°.

Table 2. Capacitances (C2) calculated from the GCD curves (Fig. 4) for the sample under different bending angles.

Bending angle,°	C2, F	Percentage, %
0	0.622	100
30	0.379	61.0
60	0.468	75.3
90	0.464	74.7
120	0.441	71.0
150	0.416	66.8

3.2.3 Comparison of the CV and GCD testing results

Capacitances C1 and C2 calculated from the CV curves and GCD curves of this strip supercapacitor under different bending conditions are shown in Fig. 5. It can be seen that C1 and C2 have little difference, which had also been proved in the reproducibility tests. They decreased dramatically when the original sample was bended to 30°. When the bending angle further increased to

60°, 90°, 120° and 150°, the capacitance changed slightly. The reason for the capacitance change under bending conditions could be a resistance increase caused by the contact changes between each part (such as electrode, current collector and separator) of the strip supercapacitor during the bending process. This will be studied and discussed further by the EIS tests later. The results indicate the strip supercapacitor made in this work is still functional under bending conditions, and shows a stable electrochemical performance under the bending conditions.

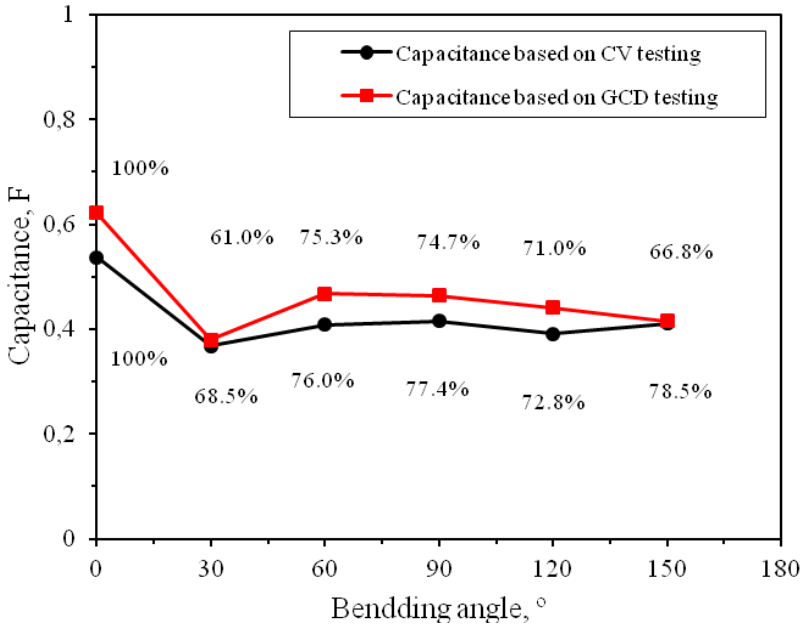

Figure 5. Capacitances calculated from CV curves (C1) and GCD curves (C2) of this strip supercapacitor under different bending angles from 0-150°.

3.2.4 EIS testing and measurement

The performance of the flexible supercapacitors under mechanical bending conditions as an important property has been studied in the related references [20-23], however, EIS testing method was not used to further study the corresponding performance in these studies. In order to find out the reason for the capacitance change for the strip supercapacitor under the bending conditions, EIS was used to further study the electrochemical performance of supercapacitors in this work.

3.2.4.1 Equivalent circuit model

Fig. 6 (a) shows the Nyquist plot and simulation of the free-standing strip supercapacitor using a 4 mV AC modulation in a frequency range of 100 kHz to 0.01 Hz. The equivalent circuit model (Fig. 6 (b)) was used for the EIS data simulation using ZView software to get the fitting parameters. In this model, CPE1 and CPE2 are the two constant phase elements, which have the impedance in the form of $Z_{CPE} = \frac{1}{Q(jw)^{\alpha}}$ (where ω is angular frequency, α is a non-dimensional number with the range of 0-1, and $j = \sqrt{-1}$). When $\alpha = 1$, the CPE becomes an ordinary capacitance; When $\alpha = 1$, the CPE impedance

becomes independent of frequency and is a plain resistance [24]. Rs represents the equivalent series resistance (ESR). Rct represents charge transfer resistance (CTR), and is a measure of electric charge transfer through the electrode surface. It is obvious that this equivalent circuit model fits well with the Nyquist plot measured. Therefore, this equivalent circuit model will be applied to all other Nyquit plots measured under other bending conditions.

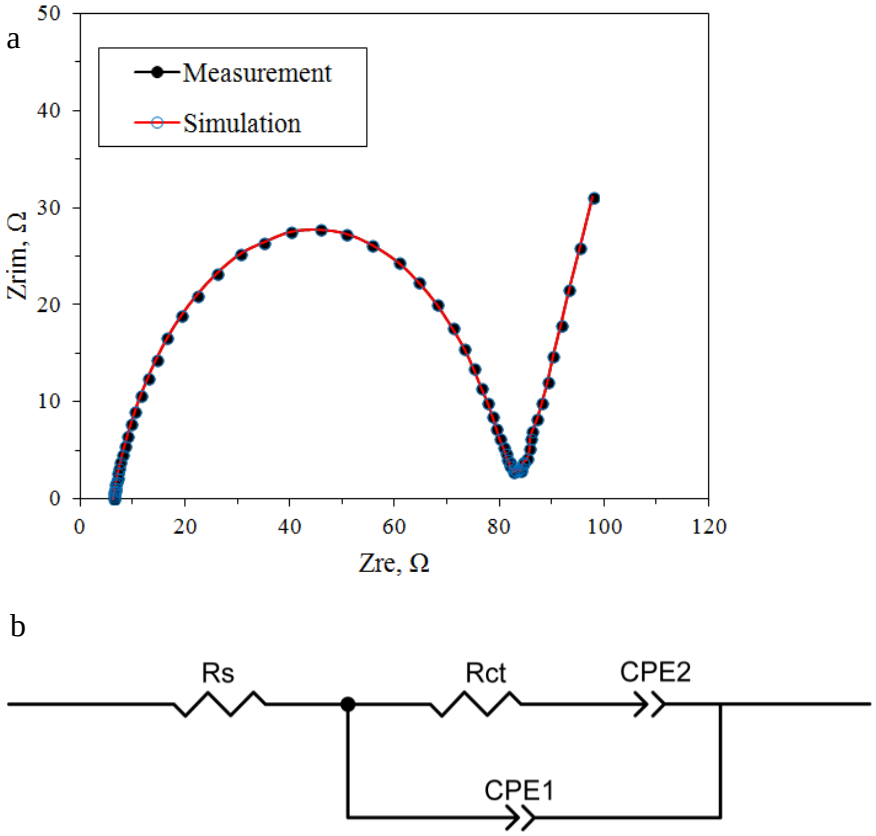

Figure 6. (a) Nyquist plot and simulation of the free-standing strip supercapacitor using a 4 mV AC modulation in a frequency range of 100 kHz to 0.01 Hz; (b) Equivalent circuit model used to fit the ac impedance data.

3.2.4.2 EIS measurement results and discussion

Fig. 7 showed the Nyquist plots of the strip supercapacitor under all different bending angles using a 4 mV AC modulation in a frequency range of 100 kHz to 0.01 Hz.

At high frequency, the ESR values of the strip supercapacitor under different bending conditions were all below 10 Ω. The resistance values were obtained from the intercept of the Nyquist plots with the real axis. It seems the ESR values of the strip supercapacitor at different bending angles changed slightly. Generally, ESR value is mainly determined by the electrolyte resistance and the contact resistance of the active material/current collector interface [25, 26]. As shown in Section 2.3, the strip supercapacitor was sealed by a laminator to protect the structure and to avoid the electrolyte leaking out. When the strip supercapacitor was under the bending conditions, the organic electrolyte cannot leak out because the whole strip supercapacitor was sealed by laminator. So the electrolyte

resistance will not change dramatically due to the total amount of the ions from the electrolyte were kept the same, resulting in only a slight change of the ESR values.

It can be seen from Fig. 7 that there is a semicircle at high frequencies for all the Nyquist plots of the strip supercapacitor tested at different bending angles. It proves that the equivalent circuit model has not been changed under bending conditions. The semicircle at high frequencies corresponds to the charge transfer limiting process, and the semicircle diameter represents the CTR, as revealed in other research [25] and [26]. It is found that the diameter of the semicircle increased approximately 24 Ω when the bending angle increased from 0° to 30°. It indicates that the CTR increased when the original sample was bended. When the bending angle increased from 30° to 60°, 90° and 120°, the diameter of the semicircle changed only slightly from 101 Ω to 106 Ω, which suggests the CTR changed slightly. It is interesting to see when the bending angle increased from 120° to 150°, the diameter of the semicircle decreased from 106 Ω to 60 Ω unexpectedly, representing the charge transfer resistance decreased about 46 Ω during this process. This might be caused by some parts of the structure distortion of the strip supercapacitor being beneficial to the charge transfer process when the bending angle increased to 150º. However, the general trend is that the CTR increased when the sample was bent.

The transition from the semicircle to the long tail can be seen in Fig. 7, which is a common phenomenon found in Nyquist plots of supercapacitors and is attributed to the ion diffusion inside the electrode [26]. Compared with the Nyquist plot of the original free-standing sample, the transitions from the semicircle to the long tail of the Nyquist plots for the sample under bending conditions are disordered. It suggests the ion diffusion inside the electrode becomes complex during the bending process. That may be caused by the differences in the dispersion of the ions in the bending region and the straight regions.

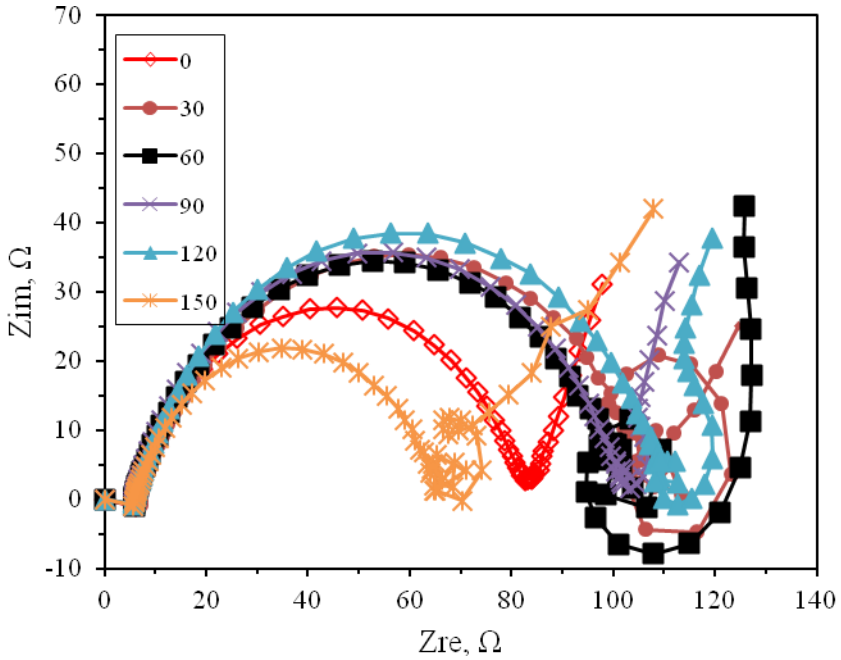

Figure 7. Nyquist plots of a strip supercapacitor under different bending conditions using a 4 mV AC modulation for a frequency range between 100 kHz to 0.01 Hz.

At each bending angle, the Nyquist plot, the CV curve and GCD curve were recorded at the same time. Because it has already been proved that there was little difference between C1 and C2, the capacitances C2 calculated from the GCD curves were used to stand for the capacitance change trend under the bending conditions. C2, as well as ESR and CTR obtained from the simulation of Nyquist Plots (Fig. 7) for the sample under different bending angles are shown in Table 3. It is noticed that when there was a significant change of the capacitance under the bending condition from 0 to 30°, e.g. the capacitance of the sample decreased from 0.622 to 0.379 F, the values of ESR and CTR changed in an opposite way, i.e. ESR increased from 6.2 to 7.0 Ω and CTR increased from 77 to 101 Ω. The reasons for the changes of the ESR and CTR values are believed to be (1) the increase of ESR caused by the contact change between the active material, the current collector, and the ion diffusion process under bending conditions; (2) the obvious increase of CTR caused by inefficiency in the charge transfer process under bending conditions. These changes of the resistance will affect the capacitance accordingly.

Table 3. Comparison of the capacitances C2, ESR and CTR under the different bending angles

Bending angle,°	Capacitance from GCD, F	ESR, Ω	CTR, Ω
0	0.622	6.2	77
30	0.379	7.0	101
60	0.468	5.8	96
90	0.464	5.7	97
120	0.441	5.9	106
150	0.416	5.9	60

4. CONCLUSIONS

In this study, the strip EDLCs were successfully designed, fabricated and characterized. The preparation process of EDLCs has a good reproducibility. These strip supercapacitors developed are still functional without shorting under bending conditions. At the initial bending at 30° there was significant change of capacitance, however, there was no significant changes found between the bending angles from 30 to 150°. Even at the large bending angle of 150°, the capacitance of the sample is still about 70% of the original capacitance for a free standing sample. Based on the simulation results of Nyquist plots the equivalent circuit model has developed. The correlation between the capacitance and the ESR and CTR was established and found that the increases of the ESR and CTR are the main reason of the capacitance decrease when the strip supercapacitor was bent. These narrow and thin strip supercapacitors which show a good flexibility have a big potential for use as a mobile energy supply.

ACKNOWLEDGEMENTS
This work was supported by the European Union Seventh Framework Programme (FP7/2007-2013) under grant agreement no. 281063.

References

1. R. Kötz, M. Carlen, *Electrochim. Acta,* 45 (2000) 2483–2498.
2. J.R. Miller, P. Simon, *Science,* 321 (2008) 651–652.
3. J. Gamby, P.L. Taberna, P. Simon, J.F. Fauvarque and M. Chesneau, *J. Power Sources,* 101 (2001) 109–116.
4. M. Jayalakshmi, K. Balasubramanian, *Int. J. Electrochem. Sci.,* 3 (2008) 1196 – 1217.
5. S. Chen, R. Ramachandran, V. Mani and R. Saraswathi, *Int. J. Electrochem. Sci.,* 9 (2014) 4072–4085.
6. Y. Zhang, H. Feng, X. Wu, L. Wang, A. Zhang, T. Xia, H. Dong, X. Li and L. Zhang, *Int. J. Hydrogen Energy,* 34 (2009) 4889–4899.
7. J. Jiang, A. Kucernak, *Electrochim. Acta,* 47 (2002) 2381–2386.
8. H. Gómez, M.K. Ram, F. Alvi, P. Villalba, E. Stefanakos and A. Kumar, *J. Power Sources,* 196 (2011) 4102–4108.
9. E. Frackowiak, Q. Abbas and F. Béguin, *J. Energy Chem.,* 22 (2013) 226–240.
10. D. Qu, *J. Power Sources,* 109 (2002) 403–411.
11. H. Shen, E. Liu, X. Xiang, Z. Huang, Y. Tian, Y. Wu, Z. Wu and H. Xie, *Mater. Res. Bull.,* 47 (2012) 662–666.
12. V.L. Pushparaj, M.M. Shaijumon, A. Kumar, S. Murugesan, L. Ci, R. Vajtai, R.J. Linhardt, O. Nalamasu and P.M. Ajayan, *Proc. Natl. Acad. Sci. U. S. A.,* 104 (2007) 13574–13577.
13. J. Bae, M.K. Song, Y.J. Park, J.M. Kim, M. Liu and Z.L. Wang, *Angew. Chemie Int. Ed.,* 50 (2011) 1683–1687.
14. M. Kaempgen, C.K. Chan, J. Ma, Y. Cui and G. Gruner, *Nano Lett.,* 9 (2009) 1872–1876.
15. K. Wang, W. Zou, B. Quan, A. Yu, H. Wu, P. Jiang and Z. Wei, *Adv. Energy Mater.,* 1 (2011) 1068–1072.
16. R. Zhang, Y. Xu, D. Harrison, J. Fyson and D. Southee, *Int. J. Electrochem. Sci.,* 11 (2016) 675–684.
17. R. Zhang, Y. Xu, D. Harrison, J. Fyson, F. Qiu and D. Southee, *Int. J. Autom. Comput.,* 12 (2015) 43–49.
18. C. Raj, B. Kim, B. Cho, W. Cho, S. Kim, S. Park and K. Yu, *Bull. Mater. Sci.,* 39 (2016), 241-248.
19. W. Xing, C. Huang, S. Zhuo, X. Yuan, G.Q. Wang, D. Hulicova-Jurcakova, Z.F. Yan and G.Q. Lu, *Carbon.,* 47 (2009), 1715-1722.
20. L. Yuan, X.H. Lu, X. Xiao, T. Zhai, J. Dai, F. Zhang, B. Hu, X. Wang, L. Gong, J. Chen, C. Hu, Y. Tong, J. Zhou and Z.L. Wang, *ACS Nano,* 6 (2012) 656-661.
21. X. Xiao, X. Peng, H. Jin, T. Li, C. Zhang, B. Gao, B. Hu, K. Huo and J. Zhou, *Adv. Mater.,* 25 (2013) 5091-5097.
22. P. Yang and W. Mai, *Nano Energy.,* 8 (2014) 274-290.
23. Y. Xu, Z. Lin, X. Huang, Y. Wang, Y. Huang and X. Duan, *Adv. Mater.,* 25 (2013) 5779-5784..
24. S. Mohammad, R. Niya and M. Hoorfar, *Electrochim. Acta,* 188 (2016) 98–102.
25. W. Cai, T. Lai, W. Dai and J. Ye, *J. Power Sources,* 255 (2014) 170–178.
26. B.G. Choi, J. Hong, W.H. Hong, P.T. Hammond and H. Park, *ACS Nano,* 5 (2011) 7205–7213.